

# EXPERIMENTAL SPACE DEBRIS SIMULATION AT EMI'S CALIBRE 4 MM TWO-STAGE LIGHT GAS GUN

Robin Putzar and Frank Schaefer

*Fraunhofer Institute for High-Speed Dynamics, Ernst-Mach-Institut, Eckerstr. 4, 79104 Freiburg, Germany*

## ABSTRACT

Reducing the vulnerability of spacecraft against space debris impact requires a thorough understanding of the processes involved in such collisions. This understanding can be gained from the analysis of laboratory experiments using accelerators capable of simulating space debris impacts at the highest velocities currently achievable on Earth. At Fraunhofer EMI, a number of two-stage light gas guns are available that are capable of reaching, depending on the gun, more than 9 km/s with relevant projectile sizes. This paper focuses on the calibre 4 mm two-stage light gas gun, which features a great number of diagnostic methods at target side, including accelerometers, force and pressure gauges, high-speed high-resolution spectroscopy and optical high-speed photography and video. The accelerator is described, and an overview on instrumentation available to systematically measure the occurring phenomena is given.

Key words: hypervelocity impacts; spacecraft protection; spacecraft vulnerability.

## 1. INTRODUCTION

Micrometeoroid and space debris (MMSD) particles pose a significant threat to manned as well as unmanned spacecraft. Small particles with sizes in the micrometre regime can degrade components located on the spacecraft surface [1, 2, 3]. Particles with sizes of one or two millimetres can perforate typical unmanned spacecraft structure walls and subsequently damage or destroy components inside [4, 5, 6, 7]. Depending on the components relevance, this can already lead to termination of a mission as reported in [8]. Impacts of larger fragments lead to disintegration of spacecraft parts [9, 10] or the whole spacecraft [11].

### 1.1. Penetration of Structure Wall vs. Functional Damage to Equipment

The current approach to quantify the threat to spacecraft posed by MMSD particles is to evaluate the probability of no penetration (PNP) of the structure wall. For

manned pressurised modules, this approach is justified by safety and operational considerations taking into account the presence of crew onboard.

The perforation of an unmanned spacecraft's external structure does not necessarily endanger the mission, since the mechanical strength of the structure is not a concern when in orbit. An exception is the case of exposed key equipment such as pressure vessels, for which an impact-induced burst will lead to termination of the mission as well as contribute to space debris generation and pollution of key orbits. Since a spacecraft's key equipment is often located behind a structure wall, a more favourable approach to define the threat posed by MMSD particles is to evaluate the risk of functional damage to such equipment, as already done for example in military aircraft risk analysis.

As this approach takes into account the intrinsic protection capabilities of the equipment, the threat to a specific configuration posed by MMSD particles is assessed lower as with the current approach. Thus if functional damage to equipment instead of penetration of the structure wall is evaluated during the design phase of a spacecraft, equivalent or better shielding capabilities can be achieved with less structural mass. The reduced mass can be utilised e. g. to decrease the overall spacecraft mass, saving launch cost. Another option is to retain the overall mass budget and increase the mass of other components, e. g. fuel, which could result in a longer operational lifetime of the spacecraft.

### 1.2. Assessing Equipment Vulnerability

To evaluate the risk of functional damage to a spacecraft's equipment, a quantification of the equipment vulnerability is required. This equipment vulnerability is a function of the threat posed by the MMSD environment and the spacecraft configuration. A comprehensive look at the vulnerability of different spacecraft subsystems is necessary to define the limit between tolerable damage and failure.

To quantify the vulnerability of spacecraft structures to micrometeoroid and space debris impacts, hypervelocity impact tests are required. A number of such impact tests

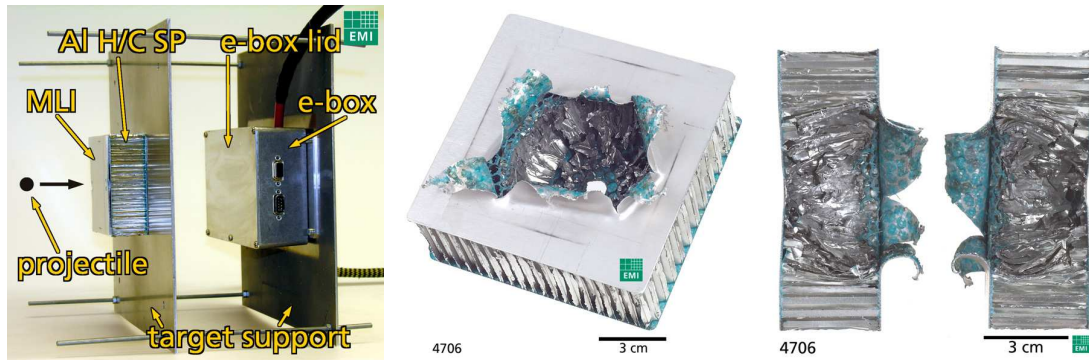


Figure 1. Example impact test on electronics. Experimental set-up (left) and rear (centre) and cut (right) view of the damaged structure wall.

were conducted during a study performed in framework of a European Space Agency Contract [12]. Results of this test campaign are reported in [4, 5, 6, 7, 13, 14].

As an example, an impact test on electronics performing simple operations is presented here. The experiment is described in detail in [5]. The experimental set-up is shown in figure 1 (left). In this experiment, a diameter 4.5 mm aluminium sphere impacted and penetrated a representative structure wall at 6.2 km/s, see figure 1 (centre and right). The structure wall consisted of an aluminium honeycomb sandwich panel (Al H/C SP) with multi-layer insulation (MLI) attached to the front. The hole diameters are 8.5 mm in the front face sheet and  $\sim 60$  mm in the rear face sheet.

The *mechanical damage* to the equipment (shown in figure 2) consists of a single perforation hole in the lid and some metallic spray on the printed circuit board. The hole in the lid is located approx. 15 mm below the impact centre and has a diameter of 0.8 mm. The metallic spray on the PCB is confined to a circle having a diameter of 17 mm.

The *functional damage* to the equipment is limited to a temporary malfunction observed during impact. The equipment suffered no permanent damage. During impact, the electronics interrupted its work 0.68 ms after impact, and automatically restarted 40 ms later. Figure 3 shows some signals recorded during the experiment.

This experiment demonstrates that there is a difference between perforation of the structure wall and mechanical damage to the equipment. The impact conditions are far above the ballistic limit of the structure wall (which is around 0.65 mm around 7 km/s), but close to the ballistic limit of the e-box lid (a similar experiment with a slightly smaller projectile – diameter 4.0 mm aluminium sphere at 6.6 km/s – resulted in no perforation of the lid but one detached spallation).

The experiment also demonstrates that there is a difference between mechanical damage and functional damage to the equipment. The decision on how much functional

damage can be tolerated by a specific equipment device can also depend on the criticality of the equipment. A temporary malfunction might be tolerable for equipment that is not vital for spacecraft survival. For key equipment such as attitude and orbit control or communication, probably a smaller risk of malfunction will be tolerated.

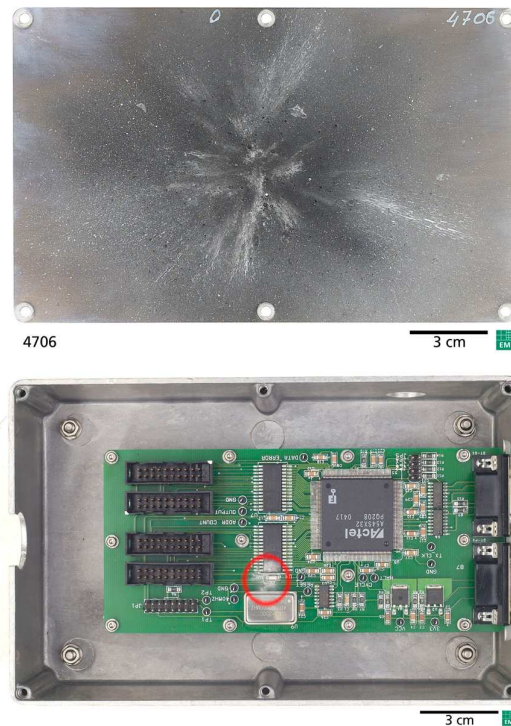


Figure 2. Example impact test on electronics. Mechanical damage to equipment: casing lid (top) and PCB (bottom).

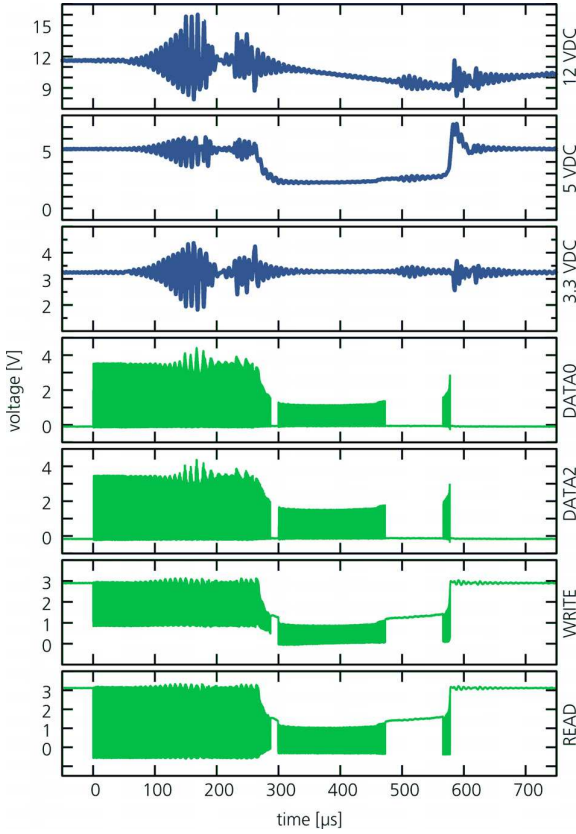


Figure 3. Example impact test on electronics. Signals of electronics recorded during the experiment.

This impact, if happened onboard a real spacecraft, would most likely be characterised as an operational anomaly. According to the current approach of risk analysis, such an impact would be counted as penetration of the structure wall and associated with a potentially critical damage to the spacecraft.

### 1.3. Reducing Equipment Vulnerability

An assessment of the individual vulnerability of equipment will lead to identification of the most vulnerable equipment. Thus besides the design of more robust spacecraft structure walls, a logical next step to increase the survivability of a spacecraft would be to harden its equipment. Reducing equipment vulnerability requires a thorough understanding of the processes involved in such collisions. This understanding can be gained from the analysis of laboratory experiments using accelerators capable of simulating space debris impacts at the highest velocities currently achievable on Earth.

### 1.4. Facilities

Fraunhofer EMI operates a number of two-stage light gas guns that differ in launch tube calibre and maximum attainable velocity. The Space Light Gas Gun, for example, is capable of accelerating projectiles having a diameter up to a few millimetres to above 9 km/s, while the Extra Large Light Gas Gun XLLGG can accelerate sabots with a calibre up to 60 mm.

This paper focuses on the calibre 4 mm two-stage light gas gun, called Baby Light Gas Gun or BLGG. However, many of the highlighted aspects are also valid for the other two-stage light gas guns operated at Fraunhofer EMI.

## 2. FACILITY DESCRIPTION

### 2.1. Working Principle

The Baby Light Gas Gun, or BLGG, is based on the two-stage light gas gun principle [16, 17]. The corresponding acceleration cycle is outlined in figure 4.

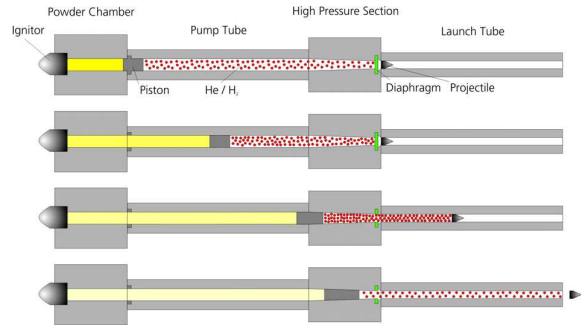


Figure 4. The two-stage light gas gun acceleration cycle.

Two-stage light gas guns drive their projectiles using gas. As with all gas driven accelerators, a part of the driver gas is accelerated to a similar velocity as the projectile. Conventional guns use the combustion gases as driver, that consist of  $\text{CO}_2$ ,  $\text{CO}$ ,  $\text{H}_2\text{O}$ ,  $\text{N}_2$  and  $\text{H}_2$  for a nitrocellulose based propellant. The kinetic energy of the gas  $E_{\text{kin}}$ , which is defined by

$$E_{\text{kin}} = \frac{1}{2}m \cdot v^2 \quad , \quad (1)$$

can only be reduced by changing the mass of the gas  $m$ , as the gas velocity  $v$  is given through the desired muzzle velocity. The molecular weight of the gases listed above is up to 44 g/mol for  $\text{CO}_2$ . Thus for high velocity shots, a considerable amount of the energy available is spent to accelerate the driver gas. In light gas guns, a gas with low molecular weight is used to drive the projectile, i. e. either  $\text{H}_2$  or  $\text{He}$ . This allows for much higher muzzle velocities (above 9 km/s for relevant projectile sizes) com-

pared to what is achievable using conventional powder guns (about 3 km/s).

The acceleration cycle essentially comprises compression of the light gas in the pump tube through a piston (first stage), and then utilising this highly compressed gas to accelerate the projectile (second stage). The piston is either driven by propellant gases (e. g. from a nitrocellulose propellant), or by a high-pressure gas from a reservoir (e. g. nitrogen). In the high pressure section, pressures above 1 GPa (10 kbar) are reached. A diaphragm is often used to seal the launch tube from the pump tube and prevent early acceleration of the projectile.

## 2.2. Gun Characteristics

The gun is shown in figure 5, a schematic sketch is shown in figure 6.



Figure 5. The Baby Light Gas Gun.

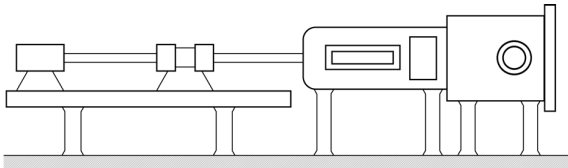


Figure 6. Schematic sketch of the Baby Light Gas Gun.

The pump tube has a length of 0.9 m and an inner diameter of 20 mm. The launch tube has a length of 0.8 m with an inner diameter ranging from 4 mm up to 6 mm. The gun is equipped with a number of sensors to allow for an investigation of the two-stage light gas gun acceleration process and calibration of numerical codes.

Using this gun, single projectiles with sizes from 0.6 mm up to 3.0 mm can be accelerated. Currently, muzzle velocities of 7 km/s have been achieved. Smaller projectiles can be accelerated as particle ensembles, i. e. several hundred particles are accelerated at the same time. Using this

technique, projectiles with diameters as low as 0.1 mm have been accelerated successfully at the BLGG.

The blast tank has four long windows (0.5 m) along the shot axis, allowing for optical diagnostics of the sabot separation process. A high-speed camera is installed together with a flash light, providing shadowgraph images as shown in figure 7. The camera is exposed twice so that the projectile's velocity can be measured close to the launch tube.

The target chamber is made of stainless steel, having an inner diameter of 0.5 m and an inner length of 0.5 m. A rotary slide pump and a turbo molecular vacuum pump are connected to the target chamber, allowing evacuating down to  $10^{-4}$  mbar.

To measure the projectile velocity, two independent systems are installed: a flash light detector that triggers upon muzzle and impact flash, and two laser light barriers integrated into the blast tank.

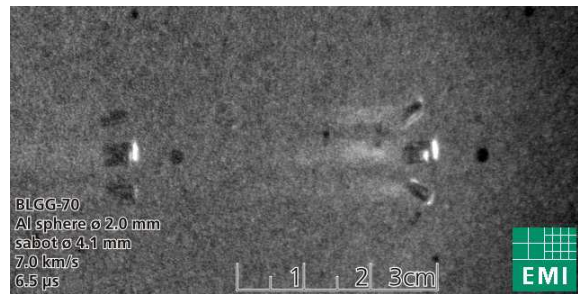


Figure 7. Sabot separation process. Image is exposed twice to allow for a velocity calculation.

## 2.3. Versatility

Using two-stage light gas guns, a great variety of projectiles can be accelerated. For micrometeoroid and space debris simulation, mainly spheres made of aluminium are used. The influence of non-spherical shapes was also investigated using two-stage light gas guns, e. g. by [18] and [19].

At the institute, a number of two-stage light gas guns are available with launch tube calibres ranging from 4 mm to 60 mm. The sabot technique used with two-stage light gas gun also offers the opportunity to investigate much more irregularly shaped projectiles, e. g. kinetic energy penetrators and models of larger objects, as the Apollo capsule shown in figure 8.

## 3. TARGET INSTRUMENTATION

At target side, a great number of diagnostic methods are available, including (but not limited to) accelerometers,

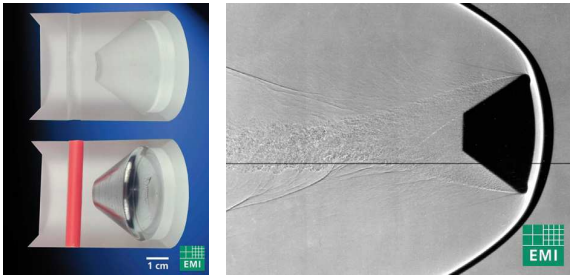


Figure 8. Sabot (left) and optical shadowgraph (right) of a model of the Apollo capsule.

force and pressure gauges, high-speed high-resolution spectroscopy and optical high-speed photography and video. All instrumentation is movable and can be used at any of the Institute's accelerators.

All diagnostic methods are utilised as required by the customer for his specific test campaign. Further diagnostic methods can be incorporated if requested by the customer.

### 3.1. Accelerometers

Two types of acceleration sensors are available at Fraunhofer EMI. For one, general purpose accelerometers are available that can be attached to various locations of the target. Such accelerometers can measure accelerations in the order of 50 000 g with a bandwidth of 10 kHz.

For tests that require high frequencies and high accelerations to be measured, a single-point laser vibrometer is available. This device can measure acceleration, velocity and displacement up to  $94 \cdot 10^6 \text{ m/s}^2$  (9.6 million g), 10 m/s and 163 mm, respectively, with frequencies up to 1.5 MHz. For lower frequencies and lower velocities, the displacement resolution can be below 100 nm. Another advantage of this device is that the only mass added to the target is a small piece of reflective foil.

Both acceleration sensors were used e. g. by Ryan [20] and Schäfer [21].

### 3.2. Pressure Gauges

A great number of pressure gauges is available at the institute to measure the pressure inside the target, e. g. pressure vessels or fuel pipes and heat pipes as reported by e. g. Putzar [6] and Schäfer [7]. Sensors based on different measurement principles are available, e. g. piezoceramic and piezoresistive.

### 3.3. High-resolution High-speed Spectroscopy

To investigate the radiation emitted during a hypervelocity impact, a high-resolution spectrometer with high-speed streak camera is available (figure 9). The resolution of the spectrometer is better than 0.5 nm, depending on the configuration. The temporal resolution of the streak camera is better than 2 ps.

Figure 10 shows a sample spectrum from a 4 mm diameter aluminium sphere impacting an aluminium sheet at 5.6 km/s in vacuum.



Figure 9. Spectrometer (left) and streak camera (right).

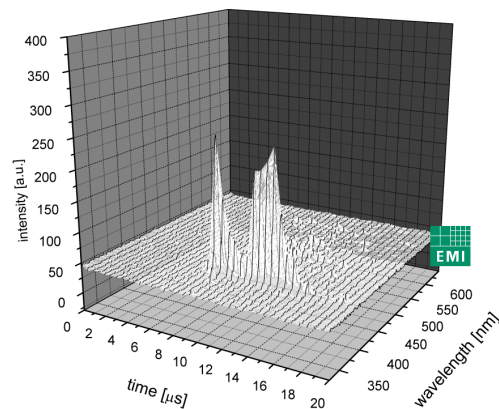


Figure 10. Example time resolved high-speed spectrograph from a 4 mm Al sphere impacting an Al sheet at 5.6 km/s in vacuum.

### 3.4. High-speed Photography and Video

A great variety of optical high-speed imaging systems are available at the institute. They are employed according to experimental requirements. The fastest camera available can record up to eight images with an interframe time down to 5 ns (up to 200 million frames per second) with shutter times down to 5 ns. For slower processes, high-speed video cameras are available with up to 675.000 frames per second with shutter times down to 1  $\mu\text{s}$ . The images can be used for analysis purposes as shown e. g. by Putzar [4]. Figure 11 shows examples

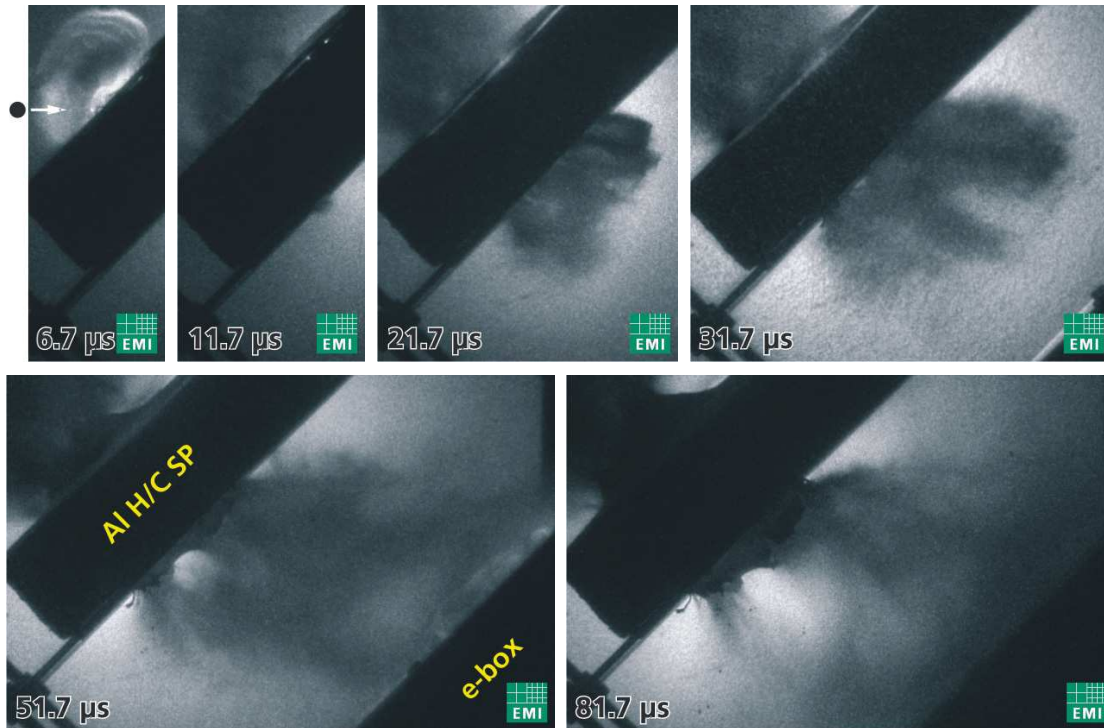


Figure 11. Sample high-speed imaging (time is with respect to impact on Al sandwich panel see [5] for details).

of a digital high-speed imaging sequence obtained during the impact of a 4.5 mm diameter aluminium sphere impacting a shielded electronics box at 6.6 km/s and 45° incidence (experimental details published in [5]).

### 3.5. Signal Recording

To record electrical signals, a number of oscilloscopes and transient recorders are available at Fraunhofer EMI, featuring high bandwidth (up to 2.5 GHz analogue bandwidth with 20 GS/s) or high vertical resolution (up to 14 bits). These devices can be used to record sensor signals from e. g. charge amplifiers for acceleration and pressure transducers, but also to directly record the signals from electronic components under investigation as presented in [4] and [5].

## 4. CONCLUSIONS

The preferred approach to evaluate risk posed by the micrometeoroid and space debris (MMSD) environment is to evaluate the functional damage to equipment caused by an impact of an MMSD particle, rather than evaluating the probability of no penetration of the structure wall. It has been demonstrated that there is a difference between perforation of the structure wall and mechanical damage to the equipment, and also between mechanical damage

and functional damage to the equipment. This difference can be exploited to reduce a spacecraft's structural mass during the design phase. To evaluate the risk of functional damage, thus to quantify the vulnerability of equipment, hypervelocity impact (HVI) tests are required.

A description of the capabilities of the calibre 4 mm two-stage light gas gun operated at Fraunhofer EMI is given. An overview on the instrumentation that is available at the Institute's guns is given. Exploitation of the target measurement readings obtained using the instrumentation described enables a systematic interpretation of the occurring phenomena. This analysis allows comprehending the interaction between MMSD particles and satellite equipment, which is important for an understanding of the failure mechanisms of individual components.

## ACKNOWLEDGEMENT

The impact experiment presented in section 1 of this paper has been conducted under ESA contract 16483/02.

## REFERENCES

- [1] Drolshagen, G., McDonnell, T., Mandeville, J.-C., & Moussi, A. 2006, Impact studies of the HST solar ar-

- rays retrieved in March 2002, *Int. J. Impact Engng* 58, 471
- [2] Edelman, K. S. 1995, Orbital impacts and the Space Shuttle windshield, *Proc. Aerospace/Defense Sensing and Dual-Use Photonics*, NASA-TM-110594
- [3] Hyde, J., Christiansen, E., Lear, D., et al. 2007, Investigation of MMOD impact on STS-115 shuttle payload bay door radiator, *Orbital Debris Quarterly News* 11, Iss. 3, 2
- [4] Putzar, R., Schäfer, F., & Lambert, M. 2008, Vulnerability of spacecraft harnesses to hypervelocity impacts, *Int. J. Impact Engng*, 35, 1728
- [5] Putzar, R., Schäfer, F., Stokes, H., Chant, R., & Lambert, M. 2006, Vulnerability of spacecraft electronics boxes to hypervelocity impacts, in *Space debris and space traffic management symposium 2005*, ed. J. Bendisch (Univelt, San Diego), 307, also published in *Proc. 56th IAC*, IAC-05-B6.4.02
- [6] Putzar, R., Schäfer, F., Romberg, O., & Lambert, M. 2005, Vulnerability of shielded fuel pipes and heat pipes to hypervelocity impacts, *Proc. 4th Europ. Conf. Space Debris*, ESA SP-587, 459
- [7] Schäfer, F. K., Putzar, R., & Lambert, M. 2008, Vulnerability of satellite equipment to hypervelocity impacts, *Proc. 59th IAC*, IAC-08-A6.3.2
- [8] Spacedaily. 2006, Russian telecom satellite fails after sudden impact, [http://www.spacedaily.com/reports/Russian\\_Telecom\\_Satellite\\_Fails\\_After\\_Sudden\\_Impact.html](http://www.spacedaily.com/reports/Russian_Telecom_Satellite_Fails_After_Sudden_Impact.html) as of 2009-03-25
- [9] Alby, F., Lansard, E., & Michal, T. 1997, Collision of cerise with space debris, *Proc. 2nd Europ. Conf. Space Debris*, ESA SP-393, 589
- [10] Sweeting, M. N., Hashida, Y., Bean, N. P., Hodgart, M. S., & Steyn, H. 2004, CERISE microsatellite recovery from first detected collision in low Earth orbit, *Acta Astronautica* 55, 139
- [11] BBC News. 2009, Russian and US satellites collide, <http://news.bbc.co.uk/1/hi/science/nature/7885051.stm> as of 2009-03-25
- [12] Putzar, R., & Schäfer, F. 2006, Vulnerability of spacecraft equipment to space debris and meteoroid impacts, Final report to ESA contract 16483/02, (Fraunhofer EMI, Freiburg, Germany), EMI-Report I-15/06
- [13] Schäfer, F., Ryan, S., Lambert, M., & Putzar, R. 2009, Improving the significance of MM/SD risk analysis by application of the SRL ballistic limit equation, *Proc. 5th Europ. Conf. Space Debris* (this volume), ESA SP-672
- [14] Schäfer, F. K., Ryan, S., Lambert, M., & Putzar, R. 2008, Ballistic limit equation for equipment placed behind satellite structure walls, *Int. J. Impact Engng* 35, 1784
- [15] Ryan, S., Schäfer, F., Destefanis, R., & Lambert, M. 2008, A ballistic limit equation for hypervelocity impacts on composite honeycomb sandwich panel satellite structures, *Advances in Space Research* 41, 1152
- [16] Crozier, W. D., & Hume, W. 1957, High-Velocity, Light-Gas Gun, *J. Appl. Phys.* 28, 892
- [17] Schneider, E. E., & Schäfer, F. K. 2001, Hypervelocity impact research: Acceleration technology and applications, *Advances in Space Research* 28, 1417
- [18] Schäfer, F. K., Herrwerth, M., Hiermaier, S. J., & Schneider, E. E. 2001, Shape effects in hypervelocity impacts on semi-infinite metallic targets, *Int. J. Impact Engng* 26, 699
- [19] Thoma, K., Schäfer, F., Hiermaier, S., & Schneider, E. 2004, An approach to achieve progress in spacecraft shielding, *Advances in Space Research* 34, 1063
- [20] Ryan, S., Schäfer, F., Spencer, G., et al. 2006, An excitation function for hypervelocity impact-induced wave propagation in satellite structures, *Proc. 57th IAC*, IAC-06-B6.3.02
- [21] Schäfer, F., Spencer, G., Ryan, S., et al. 2006, Experimental and analytical study to investigate impact-induced wave propagation in spacecraft structures, *Proc. 57th IAC*, IAC-06-B6.3.11